

# Stellar population in Active Galactic Nuclei. I. The Observations<sup>★</sup>

M. Serote Roos<sup>1,2</sup>, C. Boisson<sup>1</sup>, M. Joly<sup>1</sup>, M. J. Ward<sup>3</sup>

<sup>1</sup>*DAEC, Unité associée au CNRS et à l'Université Denis Diderot*

*Observatoire de Paris, section de Meudon*

*92195 Meudon Cedex, France*

<sup>2</sup>*Observatório Astronómico de Lisboa*

*Tapada da Ajuda*

*1300 Lisboa, Portugal*

<sup>3</sup>*X-ray Astronomy Group, Department of Physics and Astronomy*

*University of Leicester*

*Leicester LE1 7RH, England*

accepted : december 1997

## ABSTRACT

Recent observations supported by theoretical models have led to the view that giant and supergiant stars are over abundant, and/or a high metallicity component may be present, in the stellar populations at the centres of active galaxies. Here we attempt to quantify these effects by observing the strengths of the stellar absorption lines of Mg b, NaI, CaII triplet as well as molecular bands such as CN and TiO. Using long-slit spectroscopic data we are able to separate the stellar populations in and around the nucleus, for a sample including, normal, LINER, starburst and Seyfert galaxies.

In this paper we present the data, namely spectra of the nucleus and of a number of circum-nuclear regions. Comparisons reveal gradients in both the reddening and the stellar population within the central regions of most galaxies. Detailed stellar population synthesis is presented in a companion paper.

**Key words:** Galaxies: stellar content, active nuclei – methods: data analysis – methods: stellar populations

## 1 INTRODUCTION

A crucial unsolved question is whether the stellar populations in the nuclear regions of Active Galaxies differ from those of non-active galaxies of the same Hubble type. Correlations between near IR CO indices, far-infrared and X-ray luminosities of active galaxies may indicate that the more powerful monsters reside in more actively star-forming host galaxies (Yamada, 1994). The accelerated star formation caused by dynamic instabilities which trigger and/or fuel the nuclear activity could result in an overabundance of giant, supergiant and super metal rich (SMR) stars (Scoville, 1992 and references therein).

Terlevich et al. (1990) observed that in some Active Galactic Nuclei (AGN) the near IR CaII triplet absorption features are as strong, or even stronger than those of normal non-active galactic nuclei. They have suggested that

the “featureless” blue continuum previously thought to be non-stellar in origin, actually arises from the unresolved continuum from a young cluster of stars containing red supergiants. The presence of a “truly” featureless continuum is then required only in the case of some Seyfert 1 galaxies which show dilution of the CaII triplet lines. Based on independent evidence we know that in some galaxies a starburst region surrounds the unresolved nucleus which emits the broad lines e.g. NGC 7469 (Wilson et al., 1991). Nonetheless this does not prove a causal connection between the starburst and AGN.

An alternative interpretation, plausible within the framework of our knowledge of AGN, is that the stellar lines are superimposed on a non-stellar nuclear continuum, and are formed in a super metal rich population. Indeed, one could expect abundance anomalies due to the intense star formation in the metal rich environment of the nucleus.

From our detailed study of the Seyfert 1 nucleus in the galaxy NGC 3516 (Serote Roos et al., 1996), we find that the stellar population exhibits a noticeable dilution by a

<sup>★</sup> Based on observations collected at the Canadian-French-Hawaiian Telescope, Hawaii, and Observatoire de Haute Provence, France.

featureless continuum in the wavelength range 5000-9800Å as well as a high proportion of super metal rich stars.

Thus, before dismissing the possibility of the presence of any non-thermal component in the near infrared continuum of Seyfert galaxies, we must first define the stellar population in the nucleus and the surrounding regions for a sample of AGN of all levels of activity.

Until now most studies tackling this subject have made use of only a small spectral domain around a few spectral features. In order to make further progress it is necessary to extend these studies to cover more stellar absorption features, providing signatures of different stellar populations e.g. MgI  $\lambda$ 5175, NaI D  $\lambda$ 5896 and 8196Å and the numerous TiO and CN bands. The NaI lines, for example, help to distinguish between the effects of overmetallicity rather than a supergiant dominated population. Indeed, the ambiguity between metallicity and supergiant excess can be resolved by comparison of the CaII triplet and NaI absorption strengths (e.g. Zhou, 1991) although the interstellar contribution to NaI introduces some uncertainty, and also by comparison with the strength of MgI (Couture & Hardy, 1990).

In this paper we present long-slit spectroscopy, in the range 5000-9800Å of a sample of galaxies with different levels of activity. These observations are used to estimate radial gradients in the stellar population and to extract the stellar spectrum of the very nucleus. The sample is selected to include various classes of active galaxies, i.e. Seyferts 1 and 2, LINERs and starbursts, in order that the strength of the stellar features may be correlated with the general properties of each class. We also present data for two normal galaxies which will be used as comparison templates. This is not a complete sample in any statistical sense, but it does provide insights into the diversity of bulge stellar populations in and around AGN of different classes of activity.

The detailed analysis of the stellar populations for this sample using a new spectral synthesis programme (Pelat, 1997), is to be found in Paper II (Serote Roos et al., 1997).

## 2 OBSERVATIONS AND DATA ANALYSIS

The observations of 15 galaxies were carried out in January 1990, at the CFHT, Hawaii. Table 1 gives a list of the galaxies, together with their morphological type, level of activity, radial velocity, distance in Mpc (assuming  $H_0=75\text{km/s/Mpc}$  and  $q_0=0.0$ ) and colour excess due to galactic interstellar reddening. Distances have been derived from the observed emission line redshift except for the nearby galaxies NGC 3310, NGC 3379, NGC 3521, NGC 4278 and M 81 for which distances are based on published recession velocities and Virgocentric infall (Kennicutt, 1988; Bender et al., 1992). Values of  $E(B-V)$  have been evaluated using the galactic hydrogen column density derived from the 21cm survey of Stark et al. (1984) and Elvis et al. (1989).

The instrument used was the Herzberg long-slit spectrograph equipped with a 512x512 pixel CCD camera with a spatial sampling of  $0.57''/\text{px}$ . A grating of 300 lines/mm with a dispersion of  $3.3\text{Å}/\text{pixel}$  was used. The spectral resolution is  $8.5\text{Å}$  FWHM for a  $1.2''$  slit width. The seeing ranged between  $1''$  and  $1.5''$ . The slit, which has a length of 130 arcsec, was always set parallel to the parallactic angle.

The data are 2-dimensional (2D) spectra in three differ-

ent wavelength ranges: 5005-6640Å, 6585-8225Å and 8140-9785Å, with a small overlap which allows us to merge the three regions together.

The data reduction was carried out using the ESO-MIDAS package. Standard reduction procedures for bias subtraction and flat-fielding were applied. Rebinning flux onto a linear wavelength scale was carried out row by row, using the spectrum of an iron/argon calibration lamp observed before and after each exposure. The data were then corrected for airmass using the extinction curve provided in the CFHT Observer's manual. Finally, flux calibration was performed in the three wavelength ranges separately. The spectrophotometric standard stars, BD+8 2015 (Stone, 1977), HD 84937 and HD 19445 (Oke and Gunn, 1983) were observed at intervals throughout each night. The response function of the CCD was found to be uniform along the slit, so an average calibration curve was derived and applied to each row individually. A weighted mean calibration curve for each wavelength domain was constructed for each night.

Sky subtraction was then performed. By measuring the sky levels in frames of compact galaxies and stars, we determined that the sky level was uniform, i.e. no gradient was observed except for the regions closer than 40 arcsec to the edges of the frames. Therefore by restricting our analysis to data in the central 50 to 100 arcsec of the slit, no correction for sensitivity gradients along the slit need be applied. The final sky spectrum was thus the average of a number of cross-sections on both sides of the galaxies, not too far from the sampled regions. However, some of the galaxies studied have optical images extending over a few arcminutes, and hence starlight is present over the full length of the slit. But, since our integration times are relatively short and since the light profile drops rapidly, the stellar contribution from the outer regions of the galaxy is negligible. This has been confirmed by comparison of the sky spectra away from the nucleus of extended galaxies, with those of more compact galaxies. These spectra are effectively the same, implying that we do not detect starlight far away from the nucleus in any galaxy of our sample apart for M 81 which has an effective radius of 200 arcsec. In that case it was verified that absorption line equivalent width measurements, performed in spectra extracted  $\sim 30$  arcsec from the center, had the same value when sky subtraction was done using the edges of the frame than when a sky spectrum built from frames of compact galaxies was used. The only effect of weak sky contamination by the galaxy is to give final sky subtracted spectra with somewhat larger a S/N ratio.

Logarithmic flux profiles across the galaxy 2D spectra were used to determine where to extract the 1D spectra of the nucleus and the regions around it. For the nucleus we have summed between 4 and 6 rows, and for the surrounding regions between 4 and 8, depending on the seeing, the extent of the object and the S/N required. When the spectra of two symmetric regions lying on either side of the nucleus were very similar, indicating that the stellar population of the galaxy is homogeneous, we averaged them together to provide a mean spectrum. Henceforth this mean spectrum will be referred to as *the ring*, although it is long-slit data, in order to distinguish it from single region spectra. Some of the galaxies were not spatially resolved, and for these only the nuclear spectrum is presented. For nearby bright galaxies we could select up to 3 regions on each side of the nucleus.

**Table 1.** Observed galaxies.

galaxy	morphology	activity level	radial velocity (km s <sup>-1</sup> )	D Mpc	E(B-V)
NGC 1275	E cD	Seyfert 1	5264	72	0.20
NGC 2110	E3 or S0	Seyfert 2	2284	32	0.26
NGC 3227	Sb	Seyfert 1	115	12	0.03
NGC 3310	Sbc	starburst	980	19	0.01
NGC 3379	E 3	normal	920	8	0.04
NGC 3516	SB0a	Seyfert 1	2649	36	0.05
NGC 3521	Sbc	normal	805	8	0.05
NGC 4051	Sbc	Seyfert 1	725	8	0.02
NGC 4278	E1	LINER	649	9.7	0.02
NGC 5033	Sc	LINER	875	12	0.02
Mrk 3	S0	Seyfert 2	4050	56	0.13
Mrk 620	SBa	Seyfert 2	1840	24	0.09
He 2-10	dwarf Irr	starburst	873	8	0.15
MCG 8-11-11	SB	Seyfert 1	6141	80	0.32
M 81	Sb	LINER	-30	3.5	0.06

Table 2 gives the position angle of the slit, the effective radius (RC3) and the size of the regions defined along the slit for each galaxy: the fourth column gives the diameter of the nuclear region and the following columns give, on the first line the distance from the centre, and on the second line the extension, in parsecs, of each extranuclear region.

Finally, as we have no absolute flux calibration because the nights were not photometric, the median flux ratio in the overlapping region was used to normalize one segment to the next, resulting in a spectrum covering the range 5000-9780Å.

The atmospheric correction was performed with special attention, as in this wavelength range there are many strong atmospheric bands of H<sub>2</sub>O and O<sub>2</sub> which affect the metallic lines of interest for stellar population synthesis. O and B stars were observed for this purpose since they are reasonably featureless. Ideally, if one wishes to obtain good atmospheric band cancellation, one should observe an early-type star at the same airmass and quasi-simultaneously to the programme objects, since atmospheric absorption is a function of time and zenith distance. Numerous stars were observed but for practical reasons not generally at a similar airmass to the galaxies. Therefore one weighted mean and normalized atmospheric spectrum was created. The identification of the bands are mainly based on the work of Pierce & Breckinridge (1973), Vreux et al. (1983) and Wade & Horne (1988). Comparison of the strength of the O<sub>2</sub> and H<sub>2</sub>O bands in the individual spectra of the atmospheric standards showed that the relative contribution of O<sub>2</sub> and H<sub>2</sub>O vary during each night. We therefore corrected separately for O<sub>2</sub> and H<sub>2</sub>O. The 1D galaxy spectra were divided by  $[1 - (1 - atm) * K]$  where *atm* is the atmospheric O<sub>2</sub> or H<sub>2</sub>O band spectrum and *K* is a constant usually equal to 1, but which differs from unity whenever *atm* is deeper or smoother than the atmospheric bands present in the galaxy.

Figure 1 (a to o) shows the spectra extracted from the 15 galaxy frames, corrected for galactic interstellar reddening using the galactic reddening law from Howarth (1983). The spectra of the surrounding regions are displayed with

individual scaling factors chosen in order to allow the best comparison of the stellar population properties of the different regions. All spectra are displayed at rest wavelength.

Equivalent width (EW) of about 40 stellar features have been measured in almost every spectrum with the aim of performing population synthesis (see paper II). The nuclei of the Seyfert 1's and of Mrk 3, a Seyfert 2, have not been measured as they are largely dominated by emission lines. The spectra with too low signal to noise ratio to allow valuable synthesis were omitted as well. Identification and wavelength range of the absorption lines and bands, together with the measured EW can be found in the Appendix (Table A1 to 12). The ranges have been defined taking into account the shape of the absorption features in the spectra of both hot and cold stars in the stellar library. The line EW were measured using a continuum level defined over the entire wavelength range available. This method results in a more reliable determination of the line strength, compared to other methods which use only a locally defined continuum. Note that in stellar population synthesis the use of a *global* continuum is crucial, since all spectral features play a role in determining the best fit composite spectrum.

### 3 THE SAMPLE

#### 3.1 The template galaxies

The non-active galaxies in the sample are NGC 3379 (Fig. 1a) and NGC 3521 (Fig. 1b), a standard giant elliptical and a spiral galaxy respectively. No emission lines are present in any of the two galaxies. The classification of NGC 3521 as a LINER by some authors (e.g. Spinoglio & Malkan, 1989) is not supported by our data.

The nuclear spectrum of NGC 3379 is very red with strong molecular features (MgH, TiO, CN) implying a dominant cool population and significant internal reddening due to the presence of dust. The extranuclear regions of NGC 3379 (Rings 1, 2 and 3) are much bluer than the nucleus, although the molecular features are also very strong.

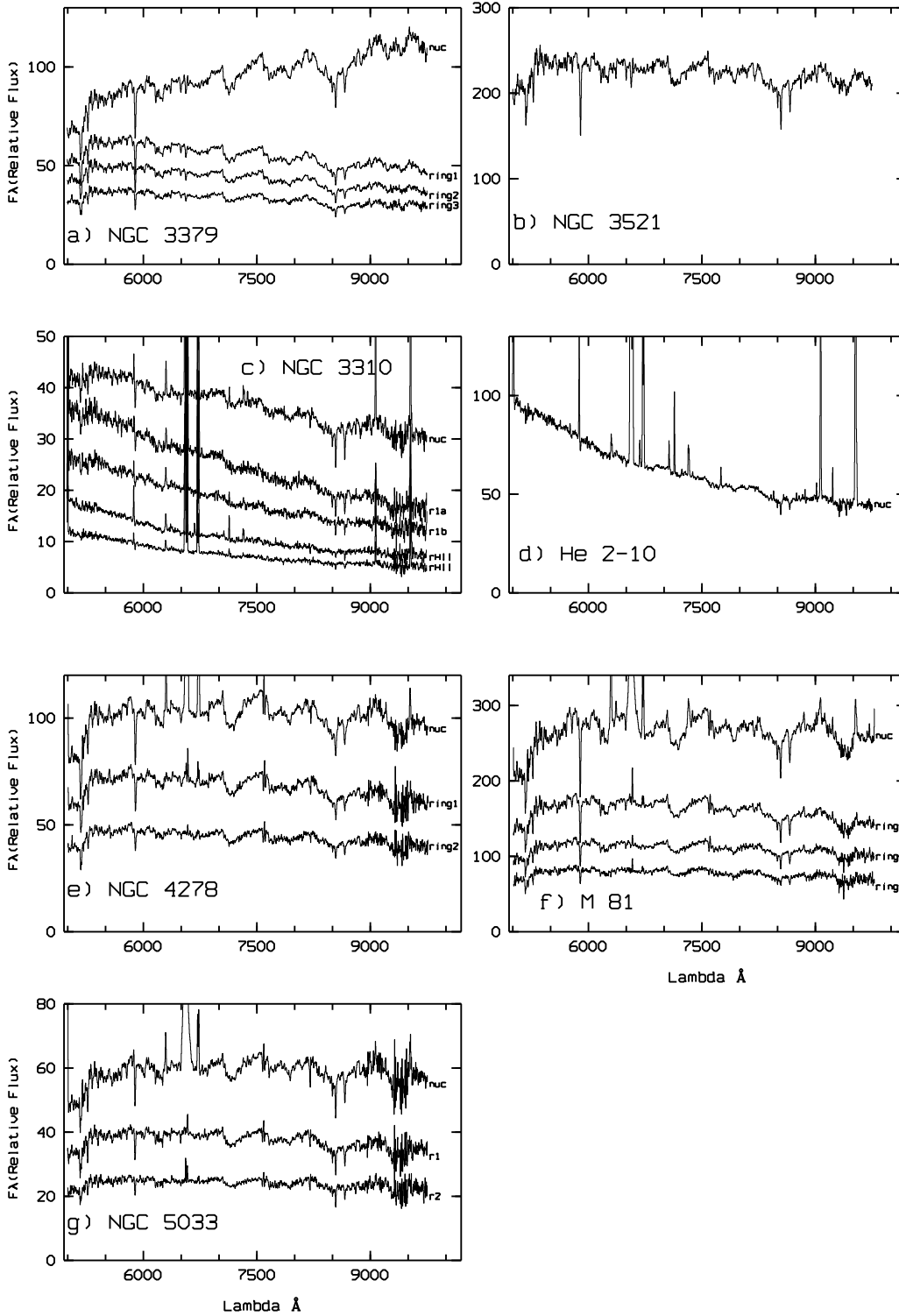


**Figure 1.** Spectra observed in the central region of a) NGC 3379. For clarity, the spectra of the off-nuclear regions have been multiplied by a scaling factor of 1.2, 2.0, 2.8, for ring 1, 2 and 3, respectively; b) Similarly for NGC 3521; c) NGC 3310: scaling factor of 2.0, 1.6, 1.0 and 1.0, for region 1a, 1b, 2a and 2b, respectively; d) He 2-10; 2) NGC 4278: scaling factor of 5.0 and 6.5, for ring 1 and 2, respectively; f) M 81: scaling factor of 1.7, 2.8, 4.2, for ring 1, 2, 3, respectively; g) NGC 5033: scaling factor of 2.2 and 3.5, for region 1 and 2, respectively.

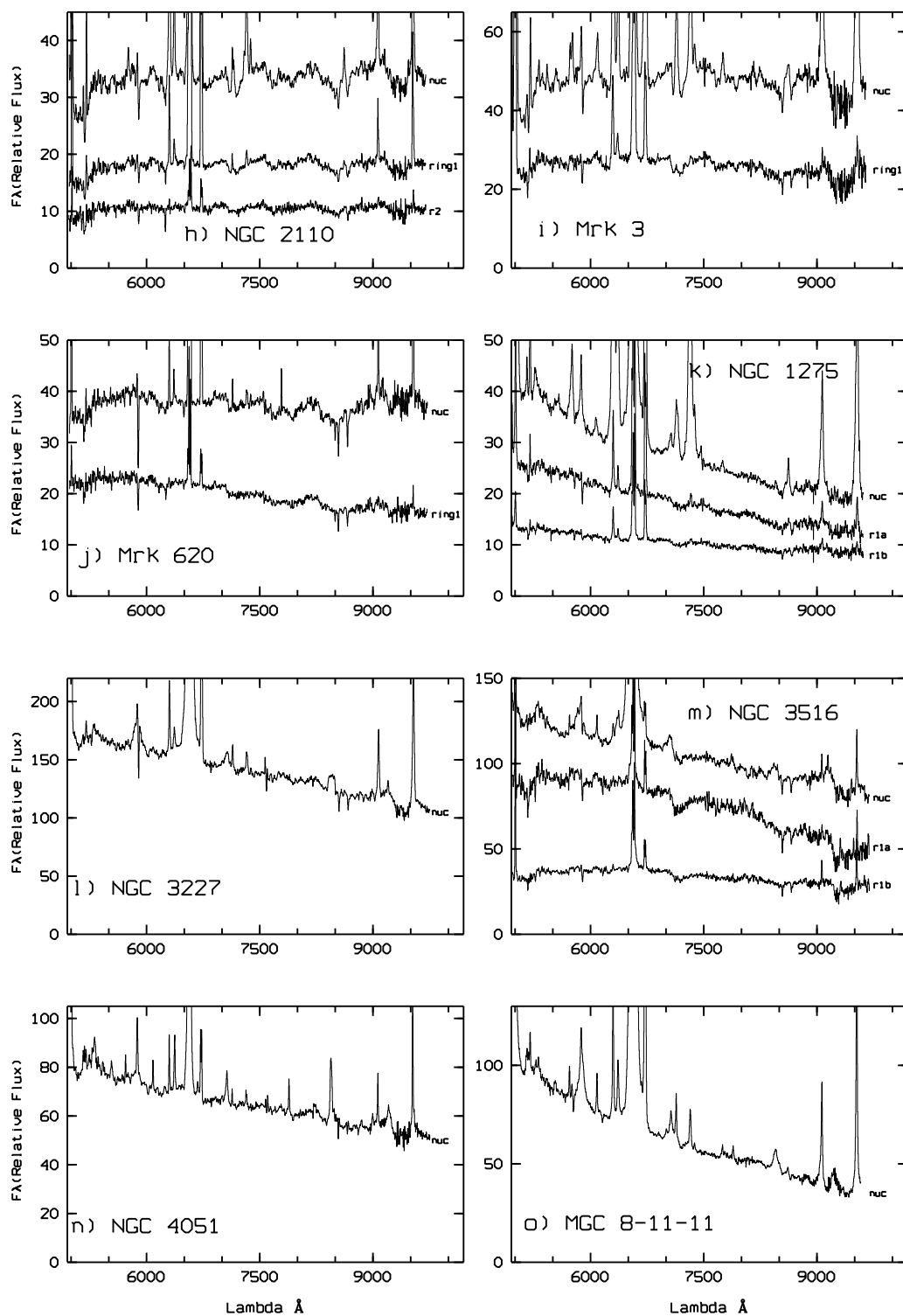


**Figure 1.** Cont. h) NGC 2110: scaling factor of 2.0 for ring 1 and region 2; i) Mrk 3: scaling factor of 2.8 for ring1; j) Mrk 620: scaling factors of 2.5 for ring 1; k) NGC 1275: scaling factors of 2.6 and 1.7, for regions 1a and 1b, respectively; l) NGC 3227; m) NGC 3516: scaling factors of 3.5; n) NGC 4051; o) MCG 8-11-11

**Table 2.** The regions defined in each galaxy

galaxy	PA ( $^{\circ}$ )	$R_e$ (kpc)	nucleus (pc)	reg1a/reg1b (pc)	reg2a/reg2b (pc)	reg3a/reg3b (pc)
NGC 1275	-30	5.9	1200	1100/1100 1000/1000	-	-
NGC 2110	-25	-	520	440(ring) 350	830/- 430	-
NGC 3227	-85	2.7	330	-	-	-
NGC 3310	-20	0.7	310	360/310 410/310	740/620 360/310	-
NGC 3379	55	2.2	110	110(ring) 110	230(ring) 130	360(ring) 130
NGC 3516	10	2.0	600	500/500 400	-	-
NGC 3521	40	2.9	400	-	-	-
NGC 4051	40	2.7	240	-	-	-
NGC 4278	-65	1.0	260	200(ring) 130	330(ring) 130	-
NGC 5033	30	4.8	230	-/210 190	-/420 230	-
Mrk 3	-10	1.4	1070	1000(ring) 930	-	-
Mrk 620	10	3.0	460	420(ring) 400	-	-
He 2-10	20	-	180	-	-	-
MCG 8-11-11	-30	-	2600	-	-	-
M 81	25	3.5	70	70(ring) 80	160(ring) 100	250(ring) 100

Our flux ratios for the three off-nuclear rings are in fair agreement with the V (Goudfrooij et al., 1994) and R (Peletier et al., 1990) surface brightness gradient. The very red nucleus (inner  $3''$ ) can be seen in the colour gradients, (B-I) and (V-I) from Goudfrooij et al. (1994). This colour gradient ( $E_{B-V}=0.26$ ) could be intrinsic to the stellar population or alternatively it could result from the presence of centrally localised dust. The fact that a dust lane (van Dokkum and Franx, 1995) has been detected, and that the spectra are similar when regions are compared to the dereddened nucleus, favours the latter hypothesis. Population gradients have been extensively studied in the central part of this elliptical galaxy. All authors agree that spectral gradients exist, but they do not agree on the slope (Davidge, 1992; Davies et al., 1993; Delisle & Hardy, 1992). In any case, gradients are steep only beyond 6 arcsec from the nucleus. Although EW are not indices a rough comparison of our measurement to published gradients can be made. The two first lines in Table A1 (labelled FeI and MgI+MgH) can be compared to the  $Mg_2$  index. If one excepts the red nucleus, that is the central 3 arcsec, only Region 3 (located beyond 6 arcsec from the nucleus) has a lower EW compared to regions 1 and 2. That is consistent with the gradient published by Davies et al. (1993). Even though FeI $\lambda$ 5270 does not show gradient some other blends of FeI, CN, CaI and

VO do. This again is consistent with the marginal variation of FeI $\lambda$ 5270 index found by Davies et al. between 3 and 9 arcsec from the center. However most absorption line EW in Table A1 display no variation from one region to the other one, and from Fig. 1a it can be seen that the circum-nuclear regions, extending from 100 to 400 pc, have remarkably similar spectra implying a very homogeneous central part.

A problem with the telescope focus, while observing NGC 3521, resulted in a defocused image and therefore precluded the possibility of obtaining spatially resolved spectra in this case. Only a spatially averaged region corresponding to 400pc in diameter could be extracted. This spectrum is similar to that extracted within the inner 10 arcsec for NGC 3379. To our knowledge no published information on colour gradients is available for NGC 3521.

### 3.2 The starburst galaxies

Spectra of two starburst galaxies, NGC 3310, a spiral, and He 2-10, a dwarf irregular, are shown in Figures 1c and d.

Compared to the normal galaxies, the nuclear spectra of the starbursts are much bluer (although the internal reddening can still be high; e.g. Hutsemekers & Surdej, 1984; Grothues & Schmidt-Kaler, 1991) and the cool old stellar component is weaker (in particular the TiO bands).

The strong emission lines characteristic of HII regions are present.

No circum-nuclear region was extracted from around the nucleus of the dwarf galaxy He 2-10 because of its low surface brightness. Johansson (1987) estimated that  $\simeq 1\%$  of the luminous mass inside 5 arcsec (150pc) of He 2-10 is in the form of newly formed stars. The emission line blend characteristic of Wolf-Rayet stars has been observed in the nucleus by Hutsemekers & Surdej (1984). In such galaxies the current rate of star formation is much higher than the average past rate. The metallicity is low (e.g. Masegosa et al., 1994; Marconi et al., 1994; Walsh & Roy, 1993).

In NGC 3310 very luminous HII regions are observed within 20 arcsec of the nucleus. These have moderately low metal abundance compared to the inner regions of galaxies of a similar Hubble type (Heckman & Balick, 1980, Pastoriza et al., 1993). This effect could be a consequence of a merger with a low metallicity galaxy (Balick & Heckman, 1981; Grothues & Schmidt-Kaler, 1991). The nucleus itself has a solar abundance (Pastoriza et al., 1993). The circum-nuclear region of NGC 3310, located around 330pc from the centre (Region 1a and 1b), is even bluer than the nucleus ( $E_{B-V}=0.25$ ). When the continua are scaled up to the same level, it can be seen that the stellar spectra are identical on both sides of the nucleus showing a weak cool stellar component and the same emission lines are present in the nucleus. The two farther regions (Region 2a and 2b) are contaminated by HII regions located at 740 and 620pc from the centre (see Fig. 1 in Pastoriza et al., 1993). An increase of the emission line strengths in Region 2a is observed with respect to the bulge component as it includes a significant contribution from the HII region, while Region 2b, close to another HII region, has emission line equivalent widths reduced by the bulge stellar continuum. It is clear that in NGC 3310 an intense phase of star formation is occurring over an extended region, and that this dominates over the cool stellar component.

### 3.3 The LINERs

The LINERs in our study are the Sb and Sc galaxies, M 81 (Fig. 1f) and NGC 5033 (Fig. 1g) respectively, as well as the giant elliptical NGC 4278 (Fig. 1e). NGC 5033 is sometimes classified as a Seyfert 1.9 galaxy, while Filippenko & Sargent (1985) state that its emission lines have some properties of both LINERs and Seyferts. Koratkar et al. (1995) detect a broad component in H $\alpha$  and H $\beta$  but its strength strongly depends on the estimated continuum level and on the subtraction of the stellar continuum. A spectral comparison with the other LINERs and Seyfert 1s presented here shows that the spectrum of NGC 5033 (observed in January 1990) does not exhibit noticeable Seyfert characteristics in the optical range. All three LINERs exhibit quite intense narrow emission lines in their nuclei plus weak H $\alpha$  emission in the surrounding regions.

A strong contribution from cool stars is obvious in all three galaxies. Circum-nuclear stellar populations appear quite homogeneous, that is that one can scale any region to the other one without striking difference. However, the nuclei are somewhat redder. This difference can be explained either by dust reddening in the nucleus ( $E_{B-V} \sim 0.07$ ) or

by the presence of a blue stellar component in the circum-nuclear region.

Near-IR line gradients are observed in M81 (Delisle & Hardy, 1992) but we cannot easily compare with results in Table A6, as CaIIIT and TiO have been measured in a different way both in terms of continuum and blend of lines. Colour gradients similar to what we find, the nuclear starlight being redder than the bulge some 20 arcsec away, are quoted in Keel (1989). Nevertheless, a characteristic of our spectra of M81 is the strong similarity between the different regions of the bulge (Rings 1, 2 and 3).

Colour and line index gradients have been observed in NGC 4278 by, respectively, Møller et al. (1995), and Davidge & Clark (1994) and Davies et al. (1993). Albeit we do find similar variations in the blue (below 5500Å), no strong gradient is apparent on the overall spectra. The change in continuum slope between the nucleus and circumnuclear regions can again be attributed to either nuclear dust or an additional small young component in the circum-nuclear regions.

### 3.4 The Seyfert 2 galaxies

Three Seyfert 2 galaxies are included in the sample: two early-type galaxies, NGC 2110 and Mrk 3 and an SBa, Mrk 620. Note that NGC 2110 and Mrk 3 have obscuring material close to their centres, and are suspected to hide a Seyfert 1 nucleus (Turner & Pounds, 1989; Miller & Goodrich, 1990; Tran, 1995).

The continuum spectra of these three Seyfert 2 nuclei (Fig. 1h, 1i and 1j) are flat and do not differ markedly from those of the LINERs, having strong absorption features from an integrated cool star spectrum on which are superimposed the high ionization emission lines characteristic of Seyfert 2s.

A circumnuclear ring spectrum at a galactocentric distance of  $\sim 450$  pc plus another from an external region at  $\sim 850$  pc have been extracted from the bulge spectrum of NGC 2110. When scaled, the stellar populations of these regions appear similar to that of the nucleus. The same situation is found for the spectra of the circumnuclear regions of Mrk 620 and Mrk 3, although the circumnuclear continuum shapes of these two galaxies are rather more blue than those of their nuclei ( $E_{B-V}=0.16$  and 0.08 respectively). A contribution from the extended narrow line region (ENLR) is conspicuous in all these extranuclear regions.

### 3.5 The Seyfert 1 galaxies

Five Seyfert 1 galaxies, NGC 1275 (Fig. 1k), NGC 3227 (Fig. 1l), NGC 3516 (Fig. 1m), NGC 4051 (Fig. 1n) and MCG 8-11-11 (Fig. 1o) are included in our sample. Only for NGC 3516, an SB0 galaxy, and NGC 1275, a cD, was it possible to extract a spectrum from the circumnuclear region; for the three other objects only the nuclear spectrum has sufficient S/N ratio. Although sometimes classified as a BL Lac type AGN, NGC 1275 has a nuclear spectrum similar to that of a Seyfert 1 in the wavelength range 5000-9800Å.

The five Seyfert 1 nuclei have broad emission lines superposed on a strong blue continuum spectrum. The stellar component, although detectable, is much weaker than in the other types of galaxy in our sample. This has been interpreted as due to dilution of the nuclear stellar component by

an additional featureless component, the nature of which is still the subject of debate (e.g. Malkan & Filippenko, 1983; Terlevich et al., 1990).

Serote Roos et al. (1996) have shown that the bulge of NGC 3516 is quite homogeneous with a cool stellar population similar to that found in the bulges of normal galaxies. In this paper the extent of the off-nuclear regions has been defined somewhat differently, having a smaller circum-nuclear region extracted from the 2D frame (400pc wide instead of 600pc). The extranuclear spectra extracted on either side of the nucleus were not averaged together, since one is bluer than the other. Nevertheless the conclusions drawn are essentially the same as those of Serote Roos et al. as these modifications are relatively minor.

The off-nuclear spectrum of NGC 1275 is very different from that of NGC 3516 having a bluer continuum and a moderately strong cool stellar component similar to that found in starburst galaxies. Malkan and Filippenko (1983) also found that the host galaxy of NGC 1275 is bluer than normal galaxies in agreement with Minkowski (1968) who first suggested the existence of a population of young stars.

In fact using the HST WFPC, Holtzman et al. (1992) discovered a population of young star clusters lying within 5kpc of the nucleus. Ferruit and Pécontal (1994) obtained 2D spectra of the central 10" (3.5 kpc) of NGC 1275 and detected emission lines associated with some of these star clusters. They interpreted this as evidence for continuing star formation as matter is accreted from the cooling flow. Our circum-nuclear spectra cover some of these young star clusters.

In NGC 3227 an HII type emission spectrum extending over a region of about 300pc from the nucleus suggests the presence of an extranuclear starburst (Arribas & Mediavilla, 1994).

#### 4 DISCUSSION

The contribution to the total spectral energy distribution (SED) of AGN arising from the stellar component of the underlying host galaxy, can be estimated from the strengths of absorption line strengths, by comparison with the corresponding strengths found in normal galaxies. A limitation of this method arises from the fact that *normal* galaxies have internal reddening, velocity dispersion, central stellar metallicity and population which may not necessarily be an appropriate match to the underlying stellar component at the centre of an active galaxy.

It is possible to alleviate some of the above mentioned problems by comparing the stellar absorption line strengths in the nucleus, with those in the surrounding regions of the bulge for the *same* galaxy, however this requires that no stellar population or dust gradient be present. We should point out that an excess of hot stars has the same effect on the shape of the spectra as would have a small reddening correction. When gradients are obviously present, a population synthesis of the different regions using data of the highest possible spatial resolution is needed.

In the nuclei of the Seyfert 1s, as expected, the contribution of the stellar component is not the dominant feature, only the CaII lines are conspicuous. We scaled the circum-nuclear stellar population in both NGC 3516 and NGC 1275,

to that of the nucleus, using the equivalent width ratio of a reference line, CaII 8542Å (cf. Serote Roos et al., 1996a). The equivalent widths were measured using a continuum level defined over the whole wavelength range. This method allows a better determination of the nucleus to bulge line ratio as it takes into account both the contribution of CaII and TiO, avoiding underestimation of the EWs in the cases where cool stars dominate the stellar population. In both Seyfert 1's, 65–85% for NGC 1275 and 50–65% for NGC 3516 of the continuum emission around CaII can be attributed to the host galaxy as long as one suppose that no gradients of any type is present. In those two cases a non-stellar featureless continuum can be inferred as one might expect for Seyfert 1s.

It should be added that, although gradients within a galaxy and/or very different populations from object to object are found, the global properties of the host galaxies are similar when large aperture are used (say about 10 arcsec for nearby galaxies). If one extracts the spectral energy distribution (SED) within 10 arcsec for the elliptical galaxies NGC 2110 and NGC 3379, and for the Sc galaxies, NGC 5033 and NGC 3521, there is a relationship between SED and morphological type. This is not surprising as we are studying the central regions/bulges of these galaxies and in no case are we sampling the disk. It is well established that ellipticals and the bulges of spirals have very similar optical SEDs. However, in our study we are not concerned with their global properties but rather in disentangling the nuclear component from the stellar features of the host galaxy. In this context we need good spatial resolution in order to isolate the unresolved nucleus, particularly since the effect we are looking for may be weak, apart from Seyfert 1s, and will be diluted within large apertures. On smaller scales the gradients can be important e.g. if one compares the two Sc galaxies, NGC 3310 and NGC 5033, it is obvious that they do not have the same properties. Line strengths, as e.g. MgH band or CaII, are not identical and therefore spurious dilutions would be deduced from direct comparison. This is partially due to very different effective radii, which must be taken into account.

#### 5 CONCLUSIONS

The nuclei of our sample galaxies are generally redder than the outer regions (this excludes Seyfert 1s as their nuclear spectra are dominated by strong broad emission lines). This colour gradient could either be due to dust or to stellar population gradients. In addition to dust/population gradients, the presence of a featureless continuum is inferred in a number of AGN. This component might be of non-thermal origin, plausible in Seyfert galaxies, or of stellar origin in the case of nuclear starburst activity. The extra component dilutes the strengths of the stellar absorption lines in the spectra of the nuclear regions of AGN. A detailed study of the spectral shape of the diluting component will allow us to differentiate between the two hypotheses.

A full population synthesis analysis for most of the galaxies in our sample, using a new method developed to determine unique solutions, is presented in Paper II.



## ACKNOWLEDGMENTS

M. Serote Roos acknowledges financial support from JNICT, Portugal, under grant no. PRAXIS XXI/BD/5270/95. We thank M. Caillat for the writing of the MEASURE program that we used to estimate the equivalent widths.

Zhou X., 1991, AA 248, 367

## REFERENCES

- Arribas S., Mediavilla E., 1994, ApJ 437, 149  
 Balick B., Heckman T.M., 1981, AA 96, 271  
 bibitemBender R., Burstein D., Faber S.M., 1992, ApJ 399, 462  
 Couture J., Hardy E., 1990, AJ 99, 540  
 Davidge T.J., Clark C.C., 1994, AJ 107, 946  
 Davidge T.J., 1992, AJ 103, 1512  
 Davies R.L., Sadler E.M., Peletier R.F., 1993, MNRAS 262, 650  
 Delisle, S., Hardy, E., 1992, AJ 103 711  
 van Dokkum P. G., Franx M., 1995, AJ 110, 2027  
 Elvis M., Lockman F., Wilkes B.J., 1989, AJ 97, 777  
 Ferruit P., Pécontal E., 1994, AA 288, 65  
 Filippenko A.V., Sargent W.L.W., 1985, ApJS 57, 503  
 Goudfrooij P., Hansen L., Jørgensen H.E., Nørgaard-Nielsen H. U., de Jong T., van den Hoek L.B., 1994, AAS 104, 179  
 Grothues H.G., Schmidt-Kaler Th., 1991, AA 242, 357  
 Heckman T.M., Balick B., 1980, AA 83, 100  
 Holtzman J.A., Faber S.M., Shaya E.J. et al., 1992, AJ 103, 691  
 Howarth I.D., 1983, MNRAS 203, 301  
 Hutsemekers D., Surdej J., 1984, AA 133, 209  
 Johansson L., 1987, AA 182, 179  
 Keel W.C., 1989, AJ 98, 195  
 Kennicutt R.C. Jr., 1988, ApJ 334, 144  
 Koratkar A., Deustua S.E., Heckman T., Filipenko A.V., Ho L.C., Rao M., 1995, ApJ 440, 132  
 Marconi G., Matteucci F., Tosi M., 1994, MNRAS 270,35  
 Masegosa J., Moles M., Campos-Aguilar A., 1994, ApJ 420, 576  
 Miller J.S., Goodrich R.W., 1990, ApJ 355, 456  
 Minkowski, R., 1968, AJ 73, 836  
 Møller P., Stiavelli M., Zeilinger W.W., 1995, MNRAS 276, 979  
 Oke J.B., Gunn J.E., 1983, ApJ 266, 713  
 Pastoriza M.G., Dottori H.A., Terlevich E., Terlevich R., Diaz A.I., 1993, MNRAS 260, 177  
 Pelat D., 1997, MNRAS 284, 365  
 Peletier R.F., Davies R.L., Illingworth G.D., Davis L.E., Cawson M., 1990, AJ 100, 1091  
 Pierce A.K., Breckinridge J.B., 1973, KPNO Contribution no.559, "The Kitt Peak table of photographic solar spectrum wavelengths"  
 Scoville, N., 1992, Relationships between active galactic nuclei and starbursts galaxies, ASP Conf. Series, vol. 31, 159  
 Serote Roos M., Boisson C., Joly M., Pelat, D., 1997, MNRAS subm. Paper II  
 Serote Roos M., Boisson C., Joly M., Ward M.J., 1996, MNRAS 278, 897  
 Spinoglio L., Malkan M.A., 1989, ApJ 342, 83  
 Stark A.A., Heiles C., Bally J., Linke R., 1984 Bell Lab. (privately distributed tape)  
 Stone R.P.S., 1977 ApJ 218, 767  
 Terlevich, E., Diaz, A.I., Terlevich, R., 1990, MNRAS 242, 271  
 Terndrup, D.M., Davies, R.L., Frogel, J.A., DePoy, D.L., Wells, L.A., 1994, ApJ 432, 518  
 Tran, H.D., 1995, ApJ 440, 578  
 Turner T.J., Pounds K.A., 1989 MNRAS 240, 858  
 Vreux, J.M., Dennefeld, M., Andriolat, Y., 1983, AAS 54, 437  
 Wade, R.A., Horne, K., 1988, ApJ 324, 411  
 Walsh J.R., Roy J.R., 1993, MNRAS 262,27  
 Yamada T., 1994 ApJ 423, L30

**APPENDIX A: ABSORPTION LINE MEASUREMENTS**

The equivalent widths (EW) presented here were measured with respect to a global continuum (see section 2). Positioning the continuum is however somewhat subjective as stellar features can be heavily blended and emission lines can be present. Consequently the errors on the EW are not simple to evaluate. One should consider both the signal to noise ratio of individual spectra and EW differences between the lowest and the highest acceptable continuum level. The latter uncertainty amounts to  $0.4\text{\AA}$  for most features. However, it can vary up to  $1\text{\AA}$  in the case of shallow features as CN. Actually this error is dominating over all other measurement and statistical uncertainties.

Column 1 of Table A1 to 12 gives the line identification of the features. Column 2 displays the wavelength ranges used to measure the EW. The EW measured in the nucleus and the circum-nuclear regions are given in the following columns. Whenever the emission lines dominate a measured wavelength range the value of the EW is omitted from the table.

**Table A1.** NGC 3379

identification	$\lambda$ ( $\text{\AA}$ )	nucleus	ring 1	ring 2	ring 3
FeI	5058-5156	21.7	19.0	19.2	18.8
FeI,MgI+MgH	5156-5240	20.3	18.5	18.3	17.7
FeI	5240-5308	7.2	6.5	6.3	6.5
FeI	5308-5356	2.5	2.2	2.6	2.6
FeI	5356-5421	3.4	3.0	3.3	3.3
FeI,TiO,MgI	5421-5554	7.8	7.2	8.4	7.8
CaI,FeI,TiO	5554-5630	4.6	4.9	5.3	4.5
FeI,TiO	5630-5676	2.1	2.1	2.1	1.8
FeI,NaI	5676-5725	1.5	1.9	1.9	1.4
FeI,TiO	5725-5825	0.9	2.1	2.5	2.1
FeI,TiO,CaI	5825-5874	0.6	1.5	1.4	1.0
NaI	5874-5914	6.3	6.5	5.7	5.6
FeI,Ti,MnI	5914-6029	4.1	5.6	5.7	5.5
FeI,CaI	6029-6110	0.4	1.6	1.8	2.0
FeI	6110-6148	0.9	1.7	1.7	1.5
TiO,CaI	6148-6208	4.7	5.4	5.7	5.3
TiO,FeI	6208-6325	9.3	10.3	10.3	10.2
FeI,CaH,TiO	6325-6374	2.7	3.1	3.0	2.9
FeI,CaI	6374-6481	2.4	3.3	3.4	2.4
FeI,TiO,CaI,BaII	6481-6535	2.8	2.8	3.1	3.1
$H_{\alpha}$ ,TiO	6535-6582	2.4	3.4	3.6	3.6
FeI,TiO	6582-6622	1.7	2.1	2.2	2.2
TiO	6622-6651	1.7	2.0	1.9	2.0
FeI,TiO	6651-6690	2.8	3.0	3.1	3.0
FeI,TiO,CaI,Si	6690-6761	5.2	6.3	5.8	5.6
FeI,TiO,CaH	6761-6795	2.1	2.6	2.8	2.6
TiO,CaH	6795-6827	1.8	2.5	2.3	2.1
FeI,SiI	6969-7048	0.7	1.6	1.6	1.4
TiO	7048-7078	1.6	2.1	2.1	1.7
TiO,NiI,FeI	7078-7140	7.2	7.9	7.5	7.1
TiO,VO	7341-7377	1.0	1.6	1.3	1.3
FeI,VO	7377-7434	0.9	1.9	1.9	1.8
FeI,VO	7434-7482	0.0	0.8	0.0	0.2
FeI,VO	7482-7540	0.0	0.2	0.0	0.0
TiO,OI	7737-7823	5.3	7.0	6.5	6.8
VO,CN,FeI	7823-7888	4.0	5.4	5.2	4.6
VO,CN,FeI	7888-7970	7.5	8.7	8.0	8.1
FeI,CN	7970-8060	4.2	5.5	4.3	4.6
TiO,FeI	8411-8453	5.3	5.7	5.6	5.7
TiO,FeI	8453-8490	5.6	5.9	5.7	5.8
CaII	8490-8508	4.0	3.6	3.5	4.1
FeI,VO,TiI	8508-8527	3.2	3.9	3.9	3.4
CaII	8527-8557	7.6	7.8	7.3	7.2
FeI,VO,TiO	8557-8645	10.6	11.0	11.8	12.1
CaII	8645-8677	6.0	6.2	6.2	6.3
FeI,MgI	8677-8768	9.2	9.9	9.9	11.1
FeI,MgI	8768-8855	5.1	6.2	6.9	7.1

Table A2. NGC 3521

identification	$\lambda$ (Å)	total
FeI	5058-5156	15.3
FeI,MgI+MgH	5156-5240	15.4
FeI	5240-5308	6.4
FeI	5308-5356	1.9
FeI	5356-5421	2.4
FeI,TiO,MgI	5421-5554	5.9
CaI,FeI,TiO	5554-5630	4.1
FeI,TiO	5630-5676	2.6
FeI,NaI	5676-5725	2.2
FeI,TiO	5725-5825	2.7
FeI,TiO,CaI	5825-5874	1.2
NaI	5874-5914	7.9
FeI,Ti,MnI	5914-6029	5.9
FeI,CaI	6029-6110	2.0
FeI	6110-6148	1.8
TiO,CaI	6148-6208	5.3
TiO,FeI	6208-6325	9.6
FeI,CaH,TiO	6325-6374	3.2
FeI,CaI	6374-6481	2.7
FeI,TiO,CaI,BaII	6481-6535	3.4
$H_{\alpha}$ ,TiO	6535-6582	3.7
FeI,TiO	6582-6622	2.0
TiO	6622-6651	1.5
FeI,TiO	6651-6690	2.6
FeI,TiO,CaI,Si	6690-6761	4.7
FeI,TiO,CaH	6761-6795	1.7
TiO,CaH	6795-6827	2.0
FeI,SiI	6969-7048	1.8
TiO	7048-7078	1.4
TiO,NiI,FeI	7078-7140	6.7
TiO,VO	7341-7377	1.4
FeI,VO	7377-7434	2.0
FeI,VO	7434-7482	0.8
FeI,VO	7482-7540	0.4
TiO,OI	7737-7823	4.5
VO,CN,FeI	7823-7888	3.2
VO,CN,FeI	7888-7970	6.7
FeI,CN	7970-8060	3.8
TiO,FeI	8411-8453	5.1
TiO,FeI	8453-8490	4.8
CaII	8490-8508	3.3
FeI,VO,TiI	8508-8527	3.5
CaII	8527-8557	7.2
FeI,VO,TiO	8557-8645	9.7
CaII	8645-8677	5.7
FeI,MgI	8677-8768	8.9
FeI,MgI	8768-8855	5.0

Table A3. NGC 3310

identification	$\lambda$ (Å)	nucleus	region 1a	region 1b
FeI	5058-5156	5.8	3.6	4.2
FeI,MgI+MgH	5156-5240	6.3	6.2	5.5
FeI	5240-5308	2.5	1.8	2.3
FeI	5308-5356	0.5	0.6	1.3
FeI	5356-5421	0.1	0.5	0.0
FeI,TiO,MgI	5421-5554	0.9	3.3	2.3
CaI,FeI,TiO	5554-5630	1.0	2.3	3.7
FeI,TiO	5630-5676	0.8	1.4	2.4
FeI,NaI	5676-5725	0.0	1.3	1.6
FeI,TiO	5725-5825	-	2.2	2.7
FeI,TiO,CaI	5825-5874	-	0.6	1.0
NaI	5874-5914	1.7	2.5	3.1
FeI,Ti,MnI	5914-6029	3.0	6.3	6.3
FeI,CaI	6029-6110	1.9	3.4	3.5
FeI	6110-6148	1.5	2.6	2.7
TiO,CaI	6148-6208	4.3	5.4	5.1
TiO,FeI	6208-6325	-	-	-
FeI,CaH,TiO	6325-6374	2.0	3.0	2.4
FeI,CaI	6374-6481	3.9	6.1	4.7
FeI,TiO,CaI,BaII	6481-6535	2.8	3.6	3.2
$H_{\alpha}$ ,TiO	6535-6582	-	-	-
FeI,TiO	6582-6622	-	-	-
TiO	6622-6651	0.6	1.4	1.6
FeI,TiO	6651-6690	1.0	1.9	2.4
FeI,TiO,CaI,Si	6690-6761	-	-	-
FeI,TiO,CaH	6761-6795	0.7	1.3	2.2
TiO,CaH	6795-6827	0.5	2.2	2.1
FeI,SiI	6969-7048	-	0.8	2.8
TiO	7048-7078	-	0.9	1.2
TiO,NiI,FeI	7078-7140	1.5	3.7	3.6
TiO,VO	7341-7377	0.3	1.6	2.4
FeI,VO	7377-7434	0.5	1.5	2.3
FeI,VO	7434-7482	0.3	1.3	2.1
FeI,VO	7482-7540	0.1	0.8	1.2
TiO,OI	7737-7823	2.8	4.8	6.1
VO,CN,FeI	7823-7888	2.7	3.7	3.7
VO,CN,FeI	7888-7970	5.0	6.6	7.3
FeI,CN	7970-8060	2.7	2.5	6.2
TiO,FeI	8411-8453	3.6	4.0	4.2
TiO,FeI	8453-8490	3.7	4.1	4.2
CaII	8490-8508	3.1	3.3	2.0
FeI,VO,TiI	8508-8527	2.1	2.6	2.5
CaII	8527-8557	5.9	6.3	5.4
FeI,VO,TiO	8557-8645	5.8	8.8	8.4
CaII	8645-8677	5.0	5.7	5.1
FeI,MgI	8677-8768	5.3	7.2	7.6
FeI,MgI	8768-8855	2.3	7.3	6.1

**Table A4.** He 2-10

identification	$\lambda$ (Å)	nucleus
FeI	5058-5156	2.8
FeI,MgI+MgH	5156-5240	3.4
FeI	5240-5308	1.9
FeI	5308-5356	0.7
FeI	5356-5421	0.9
FeI,TiO,MgI	5421-5554	2.4
CaI,FeI,TiO	5554-5630	1.9
FeI,TiO	5630-5676	0.9
FeI,NaI	5676-5725	0.0
FeI,TiO	5725-5825	2.1
FeI,TiO,CaI	5825-5874	-
NaI	5874-5914	-
FeI,Ti,MnI	5914-6029	4.3
FeI,CaI	6029-6110	2.5
FeI	6110-6148	1.5
TiO,CaI	6148-6208	3.5
TiO,FeI	6208-6325	2.9
FeI,CaH,TiO	6325-6374	0.4
FeI,CaI	6374-6481	1.8
FeI,TiO,CaI,BaII	6481-6535	2.5
$H_{\alpha}$ ,TiO	6535-6582	-
FeI,TiO	6582-6622	-
TiO	6622-6651	-
FeI,TiO	6651-6690	-
FeI,TiO,CaI,Si	6690-6761	-
FeI,TiO,CaH	6761-6795	1.7
TiO,CaH	6795-6827	1.9
FeI,SiI	6969-7048	1.5
TiO	7048-7078	-
TiO,NiI,FeI	7078-7140	-
TiO,VO	7341-7377	1.2
FeI,VO	7377-7434	2.1
FeI,VO	7434-7482	1.8
FeI,VO	7482-7540	1.7
TiO,OI	7737-7823	-
VO,CN,FeI	7823-7888	2.8
VO,CN,FeI	7888-7970	5.2
FeI,CN	7970-8060	2.4
TiO,FeI	8411-8453	2.7
TiO,FeI	8453-8490	3.5
CaII	8490-8508	2.7
FeI,VO,TiI	8508-8527	2.1
CaII	8527-8557	5.1
FeI,VO,TiO	8557-8645	5.9
CaII	8645-8677	4.2
FeI,MgI	8677-8768	5.4
FeI,MgI	8768-8855	3.2

**Table A5.** NGC 4278

identification	$\lambda$ (Å)	nucleus	ring 1	ring 2
FeI	5058-5156	23.9	20.0	18.0
FeI,MgI+MgH	5156-5240	20.7	18.9	17.6
FeI	5240-5308	7.3	6.8	5.2
FeI	5308-5356	2.5	2.0	1.8
FeI	5356-5421	2.7	1.9	1.0
FeI,TiO,MgI	5421-5554	7.4	6.7	4.3
CaI,FeI,TiO	5554-5630	5.1	5.2	4.7
FeI,TiO	5630-5676	2.4	2.6	2.1
FeI,NaI	5676-5725	2.2	2.4	1.8
FeI,TiO	5725-5825	0.9	2.7	1.5
FeI,TiO,CaI	5825-5874	0.6	1.0	0.6
NaI	5874-5914	6.0	5.7	5.2
FeI,Ti,MnI	5914-6029	6.2	7.3	6.5
FeI,CaI	6029-6110	1.5	2.8	2.4
FeI	6110-6148	1.3	1.8	1.6
TiO,CaI	6148-6208	4.7	5.0	4.6
TiO,FeI	6208-6325	-	8.7	9.4
FeI,CaH,TiO	6325-6374	1.8	2.9	2.5
FeI,CaI	6374-6481	3.7	3.9	4.0
FeI,TiO,CaI,BaII	6481-6535	-	3.7	3.4
$H_{\alpha}$ ,TiO	6535-6582	-	-	2.3
FeI,TiO	6582-6622	-	-	1.8
TiO	6622-6651	1.9	1.9	2.3
FeI,TiO	6651-6690	2.9	3.2	3.6
FeI,TiO,CaI,Si	6690-6761	-	-	4.9
FeI,TiO,CaH	6761-6795	2.6	2.5	2.6
TiO,CaH	6795-6827	2.2	2.6	2.8
FeI,SiI	6969-7048	1.2	1.6	2.4
TiO	7048-7078	1.1	1.2	1.9
TiO,NiI,FeI	7078-7140	7.0	6.8	7.2
TiO,VO	7341-7377	1.4	1.7	1.5
FeI,VO	7377-7434	1.4	1.7	1.8
FeI,VO	7434-7482	0.5	1.0	0.0
FeI,VO	7482-7540	0.2	0.3	0.0
TiO,OI	7737-7823	6.4	6.9	6.8
VO,CN,FeI	7823-7888	4.9	4.7	4.9
VO,CN,FeI	7888-7970	8.2	7.7	7.5
FeI,CN	7970-8060	4.9	4.9	5.7
TiO,FeI	8411-8453	4.9	4.6	4.4
TiO,FeI	8453-8490	5.3	5.3	4.4
CaII	8490-8508	3.2	3.6	2.9
FeI,VO,TiI	8508-8527	3.4	2.9	2.9
CaII	8527-8557	6.4	6.6	6.1
FeI,VO,TiO	8557-8645	9.2	10.3	9.3
CaII	8645-8677	5.4	5.3	4.8
FeI,MgI	8677-8768	7.0	8.6	7.2
FeI,MgI	8768-8855	3.8	5.2	4.0

Table A6. M 81

identification	$\lambda$ (Å)	nucleus	ring 1	ring2
FeI	5058-5156	22.4	20.3	17.4
FeI,MgI+MgH	5156-5240	19.6	19.5	17.2
FeI	5240-5308	7.7	7.6	6.9
FeI	5308-5356	2.9	2.4	2.3
FeI	5356-5421	4.0	3.6	3.2
FeI,TiO,MgI	5421-5554	9.8	8.2	7.6
CaI,FeI,TiO	5554-5630	6.5	5.6	5.1
FeI,TiO	5630-5676	3.4	2.9	2.5
FeI,NaI	5676-5725	2.6	2.3	2.4
FeI,TiO	5725-5825	1.6	2.2	3.2
FeI,TiO,CaI	5825-5874	1.2	1.3	1.8
NaI	5874-5914	8.1	7.5	6.5
FeI,Ti,MnI	5914-6029	6.7	6.3	6.9
FeI,CaI	6029-6110	1.6	1.9	2.4
FeI	6110-6148	2.0	2.0	2.2
TiO,CaI	6148-6208	5.9	6.0	6.2
TiO,FeI	6208-6325	4.1	10.9	11.8
FeI,CaH,TiO	6325-6374	1.1	3.3	3.2
FeI,CaI	6374-6481	1.5	3.3	3.9
FeI,TiO,CaI,BaII	6481-6535	-	2.7	2.7
$H_{\alpha}$ ,TiO	6535-6582	-	-	2.1
FeI,TiO	6582-6622	-	0.1	1.8
TiO	6622-6651	-	1.7	2.2
FeI,TiO	6651-6690	3.5	2.5	3.6
FeI,TiO,CaI,Si	6690-6761	-	3.8	5.7
FeI,TiO,CaH	6761-6795	3.9	2.6	3.0
TiO,CaH	6795-6827	3.5	1.8	2.3
FeI,SiI	6969-7048	3.9	1.6	2.0
TiO	7048-7078	2.6	1.9	2.1
TiO,NiI,FeI	7078-7140	9.4	7.8	7.2
TiO,VO	7341-7377	1.7	1.6	1.6
FeI,VO	7377-7434	2.3	1.9	1.8
FeI,VO	7434-7482	1.4	0.9	-
FeI,VO	7482-7540	0.9	0.5	-
TiO,OI	7737-7823	5.6	6.2	5.9
VO,CN,FeI	7823-7888	5.0	4.6	4.6
VO,CN,FeI	7888-7970	9.7	8.9	8.4
FeI,CN	7970-8060	5.4	5.4	4.4
TiO,FeI	8411-8453	4.9	5.0	4.3
TiO,FeI	8453-8490	4.9	5.0	4.2
CaII	8490-8508	3.4	3.8	3.4
FeI,VO,TiI	8508-8527	3.3	2.8	2.4
CaII	8527-8557	6.8	6.9	6.0
FeI,VO,TiO	8557-8645	8.3	9.2	7.8
CaII	8645-8677	5.1	5.9	5.1
FeI,MgI	8677-8768	6.8	7.3	6.0
FeI,MgI	8768-8855	2.3	3.8	2.7

Table A7. NGC 5033

identification	$\lambda$ (Å)	nucleus	region 1	region 2
FeI	5058-5156	17.3	16.6	13.0
FeI,MgI+MgH	5156-5240	15.1	15.0	12.8
FeI	5240-5308	5.7	5.1	3.7
FeI	5308-5356	1.7	1.4	2.0
FeI	5356-5421	2.9	1.9	1.5
FeI,TiO,MgI	5421-5554	7.1	5.1	5.2
CaI,FeI,TiO	5554-5630	5.9	4.4	4.3
FeI,TiO	5630-5676	3.0	2.0	1.9
FeI,NaI	5676-5725	2.9	2.1	1.9
FeI,TiO	5725-5825	2.4	1.8	2.0
FeI,TiO,CaI	5825-5874	-	0.5	1.1
NaI	5874-5914	3.7	4.1	4.0
FeI,Ti,MnI	5914-6029	5.3	4.8	5.3
FeI,CaI	6029-6110	1.7	1.1	1.9
FeI	6110-6148	1.4	1.2	1.0
TiO,CaI	6148-6208	4.7	3.7	4.9
TiO,FeI	6208-6325	6.1	6.6	7.5
FeI,CaH,TiO	6325-6374	1.9	1.7	2.9
FeI,CaI	6374-6481	3.3	1.9	4.9
FeI,TiO,CaI,BaII	6481-6535	-	2.1	3.7
$H_{\alpha}$ ,TiO	6535-6582	-	-	-
FeI,TiO	6582-6622	-	-	0.8
TiO	6622-6651	-	1.0	1.3
FeI,TiO	6651-6690	1.8	1.9	2.2
FeI,TiO,CaI,Si	6690-6761	-	3.0	3.3
FeI,TiO,CaH	6761-6795	2.3	1.4	1.7
TiO,CaH	6795-6827	1.8	1.0	1.9
FeI,SiI	6969-7048	1.1	0.1	1.7
TiO	7048-7078	0.8	0.9	1.4
TiO,NiI,FeI	7078-7140	5.2	5.6	5.9
TiO,VO	7341-7377	1.0	0.9	1.6
FeI,VO	7377-7434	1.3	1.1	2.0
FeI,VO	7434-7482	-	0.0	1.0
FeI,VO	7482-7540	-	-	1.0
TiO,OI	7737-7823	3.3	4.6	6.6
VO,CN,FeI	7823-7888	2.9	3.5	4.6
VO,CN,FeI	7888-7970	6.2	5.6	8.1
FeI,CN	7970-8060	2.9	2.1	5.2
TiO,FeI	8411-8453	3.4	4.7	4.7
TiO,FeI	8453-8490	3.8	4.9	5.0
CaII	8490-8508	3.1	3.7	3.7
FeI,VO,TiI	8508-8527	3.0	2.8	3.0
CaII	8527-8557	6.1	6.7	6.9
FeI,VO,TiO	8557-8645	7.3	9.8	9.0
CaII	8645-8677	4.9	5.9	5.9
FeI,MgI	8677-8768	6.7	9.0	10.0
FeI,MgI	8768-8855	2.8	5.5	7.0

**Table A8.** NGC 2110

identification	$\lambda$ (Å)	nucleus	ring 1
FeI	5058-5156	20.1	22.6
FeI,MgI+MgH	5156-5240	-	-
FeI	5240-5308	4.9	9.3
FeI	5308-5356	1.7	4.2
FeI	5356-5421	2.3	4.2
FeI,TiO,MgI	5421-5554	6.5	8.0
CaI,FeI,TiO	5554-5630	3.6	4.0
FeI,TiO	5630-5676	2.7	3.3
FeI,NaI	5676-5725	2.0	3.0
FeI,TiO	5725-5825	-	0.7
FeI,TiO,CaI	5825-5874	0.6	1.3
NaI	5874-5914	4.1	3.3
FeI,Ti,MnI	5914-6029	6.2	5.7
FeI,CaI	6029-6110	0.1	-
FeI	6110-6148	1.4	0.7
TiO,CaI	6148-6208	4.4	3.1
TiO,FeI	6208-6325	-	-
FeI,CaH,TiO	6325-6374	-	-
FeI,CaI	6374-6481	-	-
FeI,TiO,CaI,BaII	6481-6535	-	-
$H_{\alpha}$ ,TiO	6535-6582	-	-
FeI,TiO	6582-6622	-	-
TiO	6622-6651	-	-
FeI,TiO	6651-6690	-	-
FeI,TiO,CaI,Si	6690-6761	-	-
FeI,TiO,CaH	6761-6795	3.0	2.4
TiO,CaH	6795-6827	2.7	1.8
FeI,SiI	6969-7048	1.7	1.0
TiO	7048-7078	0.9	1.1
TiO,NiI,FeI	7078-7140	3.8	4.7
TiO,VO	7341-7377	-	1.0
FeI,VO	7377-7434	-	0.7
FeI,VO	7434-7482	-	0.4
FeI,VO	7482-7540	-	-
TiO,OI	7737-7823	3.2	3.5
VO,CN,FeI	7823-7888	3.2	3.2
VO,CN,FeI	7888-7970	5.9	5.1
FeI,CN	7970-8060	2.6	1.5
TiO,FeI	8411-8453	3.5	4.0
TiO,FeI	8453-8490	4.2	4.2
CaII	8490-8508	3.3	2.8
FeI,VO,TiI	8508-8527	2.3	2.7
CaII	8527-8557	5.9	6.1
FeI,VO,TiO	8557-8645	2.6	6.4
CaII	8645-8677	4.3	4.2
FeI,MgI	8677-8768	3.6	5.8
FeI,MgI	8768-8855	0.4	1.9

**Table A9.** Mrk 3

identification	$\lambda$ (Å)	ring 1
FeI	5058-5156	16.8
FeI,MgI+MgH	5156-5240	14.4
FeI	5240-5308	5.6
FeI	5308-5356	2.0
FeI	5356-5421	4.0
FeI,TiO,MgI	5421-5554	10.4
CaI,FeI,TiO	5554-5630	6.2
FeI,TiO	5630-5676	5.4
FeI,NaI	5676-5725	5.2
FeI,TiO	5725-5825	7.0
FeI,TiO,CaI	5825-5874	2.8
NaI	5874-5914	6.4
FeI,Ti,MnI	5914-6029	7.3
FeI,CaI	6029-6110	1.3
FeI	6110-6148	2.0
TiO,CaI	6148-6208	6.2
TiO,FeI	6208-6325	-
FeI,CaH,TiO	6325-6374	-
FeI,CaI	6374-6481	-
FeI,TiO,CaI,BaII	6481-6535	-
$H_{\alpha}$ ,TiO	6535-6582	-
FeI,TiO	6582-6622	-
TiO	6622-6651	-
FeI,TiO	6651-6690	-
FeI,TiO,CaI,Si	6690-6761	-
FeI,TiO,CaH	6761-6795	2.0
TiO,CaH	6795-6827	1.7
FeI,SiI	6969-7048	1.6
TiO	7048-7078	1.7
TiO,NiI,FeI	7078-7140	8.0
TiO,VO	7341-7377	1.5
FeI,VO	7377-7434	1.8
FeI,VO	7434-7482	0.6
FeI,VO	7482-7540	0.4
TiO,OI	7737-7823	6.4
VO,CN,FeI	7823-7888	3.5
VO,CN,FeI	7888-7970	6.9
FeI,CN	7970-8060	4.2
TiO,FeI	8411-8453	6.0
TiO,FeI	8453-8490	5.6
CaII	8490-8508	3.1
FeI,VO,TiI	8508-8527	3.9
CaII	8527-8557	7.1
FeI,VO,TiO	8557-8645	10.2
CaII	8645-8677	6.0
FeI,MgI	8677-8768	8.5
FeI,MgI	8768-8855	7.5

Table A10. Mrk 620

identification	$\lambda$ (Å)	nucleus	ring 1
FeI	5058-5156	12.2	7.1
FeI,MgI+MgH	5156-5240	10.6	8.8
FeI	5240-5308	4.9	2.9
FeI	5308-5356	1.6	1.1
FeI	5356-5421	2.3	1.3
FeI,TiO,MgI	5421-5554	3.3	3.8
CaI,FeI,TiO	5554-5630	1.7	2.9
FeI,TiO	5630-5676	0.4	1.0
FeI,NaI	5676-5725	0.3	1.7
FeI,TiO	5725-5825	-	2.5
FeI,TiO,CaI	5825-5874	-	1.1
NaI	5874-5914	4.4	5.6
FeI,Ti,MnI	5914-6029	1.7	5.3
FeI,CaI	6029-6110	-	1.7
FeI	6110-6148	1.1	2.3
TiO,CaI	6148-6208	3.5	4.5
TiO,FeI	6208-6325	2.7	8.0
FeI,CaH,TiO	6325-6374	-	1.6
FeI,CaI	6374-6481	4.0	1.2
FeI,TiO,CaI,BaII	6481-6535	3.6	-
$H_{\alpha}$ ,TiO	6535-6582	-	-
FeI,TiO	6582-6622	-	-
TiO	6622-6651	1.6	-
FeI,TiO	6651-6690	1.6	-
FeI,TiO,CaI,Si	6690-6761	-	-
FeI,TiO,CaH	6761-6795	1.5	0.9
TiO,CaH	6795-6827	1.3	0.8
FeI,SiI	6969-7048	0.6	-
TiO	7048-7078	0.6	0.9
TiO,NiI,FeI	7078-7140	3.2	4.0
TiO,VO	7341-7377	1.3	1.9
FeI,VO	7377-7434	1.6	2.4
FeI,VO	7434-7482	1.2	1.4
FeI,VO	7482-7540	0.9	2.1
TiO,OI	7737-7823	-	7.5
VO,CN,FeI	7823-7888	4.8	5.1
VO,CN,FeI	7888-7970	8.1	7.9
FeI,CN	7970-8060	5.5	5.1
TiO,FeI	8411-8453	4.1	4.1
TiO,FeI	8453-8490	4.5	3.9
CaII	8490-8508	3.6	3.4
FeI,VO,TiI	8508-8527	2.9	2.3
CaII	8527-8557	6.3	6.3
FeI,VO,TiO	8557-8645	8.4	7.8
CaII	8645-8677	5.0	5.4
FeI,MgI	8677-8768	7.2	7.2
FeI,MgI	8768-8855	3.1	3.1

Table A11. NGC 1275

identification	$\lambda$ (Å)	region 1a	region 1b
FeI	5058-5156	4.3	5.0
FeI,MgI+MgH	5156-5240	5.2	4.9
FeI	5240-5308	1.6	2.2
FeI	5308-5356	0.4	0.7
FeI	5356-5421	1.3	1.9
FeI,TiO,MgI	5421-5554	5.7	6.7
CaI,FeI,TiO	5554-5630	2.8	4.1
FeI,TiO	5630-5676	1.4	2.2
FeI,NaI	5676-5725	1.7	2.8
FeI,TiO	5725-5825	2.7	4.4
FeI,TiO,CaI	5825-5874	1.8	2.0
NaI	5874-5914	4.7	3.7
FeI,Ti,MnI	5914-6029	7.9	10.2
FeI,CaI	6029-6110	4.1	5.8
FeI	6110-6148	2.2	3.1
TiO,CaI	6148-6208	4.5	6.3
TiO,FeI	6208-6325	-	-
FeI,CaH,TiO	6325-6374	-	-
FeI,CaI	6374-6481	6.7	9.6
FeI,TiO,CaI,BaII	6481-6535	-	-
$H_{\alpha}$ ,TiO	6535-6582	-	-
FeI,TiO	6582-6622	-	-
TiO	6622-6651	-	1.5
FeI,TiO	6651-6690	1.3	2.1
FeI,TiO,CaI,Si	6690-6761	-	-
FeI,TiO,CaH	6761-6795	1.5	1.6
TiO,CaH	6795-6827	1.2	1.8
FeI,SiI	6969-7048	2.0	3.1
TiO	7048-7078	1.2	1.7
TiO,NiI,FeI	7078-7140	4.7	6.3
TiO,VO	7341-7377	1.1	1.1
FeI,VO	7377-7434	1.8	2.3
FeI,VO	7434-7482	0.1	0.8
FeI,VO	7482-7540	0.2	1.4
TiO,OI	7737-7823	3.5	5.1
VO,CN,FeI	7823-7888	3.3	4.7
VO,CN,FeI	7888-7970	5.3	7.7
FeI,CN	7970-8060	3.4	5.1
TiO,FeI	8411-8453	5.4	5.0
TiO,FeI	8453-8490	5.2	5.1
CaII	8490-8508	3.6	3.4
FeI,VO,TiI	8508-8527	3.2	2.9
CaII	8527-8557	5.5	5.8
FeI,VO,TiO	8557-8645	7.8	9.6
CaII	8645-8677	5.3	5.2
FeI,MgI	8677-8768	7.6	7.6
FeI,MgI	8768-8855	2.4	4.3

**Table A12.** NGC 3516

identification	$\lambda$ (Å)	région 1	région 1b
FeI	5058-5156	12.3	16.0
FeI,MgI+MgH	5156-5240	13.6	14.5
FeI	5240-5308	4.5	6.7
FeI	5308-5356	0.9	2.8
FeI	5356-5421	2.9	3.5
FeI,TiO,MgI	5421-5554	6.7	8.3
CaI,FeI,TiO	5554-5630	5.1	6.3
FeI,TiO	5630-5676	3.2	3.4
FeI,NaI	5676-5725	2.6	3.3
FeI,TiO	5725-5825	1.1	1.7
FeI,TiO,CaI	5825-5874	0.8	0.7
NaI	5874-5914	3.8	3.8
FeI,Ti,MnI	5914-6029	8.0	6.8
FeI,CaI	6029-6110	1.6	1.1
FeI	6110-6148	1.8	1.6
TiO,CaI	6148-6208	4.1	3.0
TiO,FeI	6208-6325	7.5	-
FeI,CaH,TiO	6325-6374	2.2	1.5
FeI,CaI	6374-6481	3.5	2.5
FeI,TiO,CaI,BaII	6481-6535	-	-
$H_{\alpha}$ ,TiO	6535-6582	-	-
FeI,TiO	6582-6622	-	-
TiO	6622-6651	-	-
FeI,TiO	6651-6690	-	-
FeI,TiO,CaI,Si	6690-6761	-	-
FeI,TiO,CaH	6761-6795	2.3	0.7
TiO,CaH	6795-6827	2.6	1.0
FeI,SiI	6969-7048	3.1	1.3
TiO	7048-7078	2.1	1.6
TiO,NiI,FeI	7078-7140	8.5	7.1
TiO,VO	7341-7377	2.3	2.4
FeI,VO	7377-7434	3.0	3.1
FeI,VO	7434-7482	1.9	1.9
FeI,VO	7482-7540	2.3	2.9
TiO,OI	7737-7823	3.2	5.7
VO,CN,FeI	7823-7888	2.9	4.1
VO,CN,FeI	7888-7970	4.8	6.7
FeI,CN	7970-8060	0.8	2.5
TiO,FeI	8411-8453	5.1	4.2
TiO,FeI	8453-8490	4.6	4.0
CaII	8490-8508	3.4	3.3
FeI,VO,TiI	8508-8527	3.1	2.4
CaII	8527-8557	7.0	6.2
FeI,VO,TiO	8557-8645	10.2	7.4
CaII	8645-8677	5.3	5.0
FeI,MgI	8677-8768	9.7	5.9
FeI,MgI	8768-8855	4.6	1.1